Journal of Advances in Science and Technology
Vol. 22, Issue No. 1, March-2025, ISSN 2230-9659

DOI: https://doi.org/10.29070/osmx2w22

Check for updates

# Development of Anti-counterfeiting ink and Hydrogel with red luminous $Ca^{2+}$-Doped $Y_2O_3:Eu^{3+}$ (1 mol%) nanoparticles

**Renu [1] * , Dr. Jitender Jindal [2] , Dr. Heena Dahiya [3]**

1. Research Scholar, Baba Mastnath University, Asthal Bohar, Rohtak, Haryana, India
renutundwal5@gmail.com ,
2. Assistant Professor, Department of Chemistry, RPS Degree College, Balana, Mahendergarh, Haryana, India ,
3. Assistant Professor, Department of Physical Sciences (Chemistry), Baba Mastnath University, Asthal Bohar, Rohtak, Haryana, India

**Abstract:** A divalent calcium ion (1 mol %) co-doped with $Y_2O_3:Eu^{3+}$(1 mol %) nano-phosphors was successfully synthesized via the solution combustion method using urea as a fuel. The nanophosphor underwent structural and optical characterization via XRD, SEM, and PL techniques. X-ray diffraction confirmed a pure, highly crystalline cubic $Y_2O_3$ phase, while SEM revealed a spherical morphology with slight agglomeration. The PL data revealed that $Ca^{2+}$ co-doping significantly enhanced the red $^5D_0 \rightarrow {}^7F_2$ emission of $Eu^{3+}$ at 613 nm, indicating improved energy transfer and local symmetry. The phosphor exhibited near-ideal red CIE coordinates making it a strong candidate for solid-state lighting and display technologies. Moreover, the prepared luminous material was used to develop an anti-counterfeiting (AC) invisible ink that emits a vivid red glow under UV light. The designs were treated with several solvents, including ethanol, acetone, HCl, $NH_3$, and NaOH, which could destroy the design's foundation, in order to assess the ink's chemical stability. The digital images displayed in Fig. demonstrate the patterns' notable resistance to the solvent.

**Keywords:** Nanophosphors, AC-ink, Luminous nanomaterial, Hydrogel

X

## INTRODUCTION

Luminescent anti-counterfeiting inks have become incredibly important in a variety of international businesses in recent years. These cutting-edge inks are essential for preventing counterfeiting and guaranteeing product authenticity. Polyvinyl alcohol (PVA) is the most suitable matrix among the materials investigated for creating luminous inks. It is a very useful and adaptable media in this cutting-edge field because of its remarkable qualities, which include high optical transparency, low toxicity, water solubility, mechanical strength, biocompatibility, and good film-forming capacity [1].

Luminescent materials, such as lanthanide-doped nanomaterials, quantum dots, organic dyes, and nanoscale metal-organic frameworks, are used in a wide range of anti-counterfeiting ink formulations. Luminescent nanomaterials doped with lanthanides, especially those based on trivalent rare-earth ions ($RE^{3+}$), have become the most promising of these. Their exceptional features, which include large Stokes and anti-Stokes shifts, high quantum efficiency, clearly defined emission bands, and luminescence durations ranging from microseconds to milliseconds, are what make them appealing. Additionally, they have minimal toxicity, exceptional photostability, and excellent chemical and thermal stability. Due to their distinct electronic transitions over a wide spectrum range, $RE^{3+}$ ions are very adaptable for next-generation

anti-counterfeiting technologies, enabling customized emission from the ultraviolet (UV) to the infrared (IR) [2, 3].

In this situation, adding divalent calcium ions ($Ca^{2+}$) to the $Y_2O_3:Eu^{3+}$ system is a useful way to change the local crystal field surrounding $Eu^{3+}$ or produce more oxygen vacancies, which may increase the photoluminescence efficiency [4-7]. Furthermore, $Ca^{2+}$ co-doping can improve energy transfer and alter site symmetry, which can improve colour purity and emission intensity [8]. The synergistic effects of $Eu^{3+}$ and $Ca^{2+}$ co-doping in $Y_2O_3$ still require systematic exploration despite the abundance of research on RE-doped oxides, especially in relation to the structural, morphological, and photoluminescent properties. The need for sophisticated luminous materials that are hard to copy but simple to authenticate has increased because to the growing threat of counterfeit goods in industries including medicine, cash, and branded goods. In this regard, the crisp emission lines, long-term stability, and excitation flexibility under UV or near-UV light sources of rare-earth (RE) doped phosphors, especially $Eu^{3+}$-activated $Y_2O_3$, have demonstrated great promise [9,10]. $Ca^{2+}$ ions can be added to the $Y_2O_3:Eu^{3+}$ matrix to further customise emission characteristics and enhance quantum efficiency, which makes these materials ideal for optical tagging and secret security printing [11, 12].The creation of defect states or local symmetry alterations surrounding $Eu^{3+}$ ions, which can alter emission lifetimes and increase red emission intensity, is one of the main benefits of $Ca^{2+}$ co-doping [13].

The development of multi-layered or time-gated anti-counterfeiting inks is made possible by these adjustable optical characteristics, where the emission response under various wavelengths or time delays adds another level of complexity to authentication procedures [14]. In order to create safe, printable luminous patterns, $Ca^{2+}$ co-doped $Y_2O_3:Eu^{3+}$ nanoparticles can be distributed in ink formulations or polymeric matrix, including hydrogels. The incorporation of luminous nanophosphors for wearable authentication systems and bio-imaging markers is made possible by hydrogels, which offer a biocompatible, flexible, and transparent medium [15].Furthermore, stimuli-responsive anti-counterfeiting devices can be created by combining photoluminescent properties with the swelling behaviour and responsiveness of hydrogels to external stimuli (such as pH, temperature, moisture) [16,17].

This study focused on the development of novel $Ca^{2+}$ (1mol %) co-doped $Y_2O_3:Eu^{3+}$ (1mol %) nano-phosphors using combustion techniques. The resulting phosphor was characterized using various methods, including X-ray diffraction (XRD), scanning electron microscopy (SEM), and photoluminescence (PL). Long-term use in biocompatible applications, such as fluorescent hydrogels for biomedical sensing or diagnostics, where both visual and analytical readouts are crucial, is also made possible by the luminous stability of $Y_2O_3:Eu^{3+}$, $Ca^{2+}$ in hydrophilic settings [18]. Therefore, these nanophosphors' multifunctionality makes them promising materials for next-generation smart materials as well as covert ink technologies.

## SYNTHESIS

### Synthesis of $Ca^{2+}$ (1mol %) Co-doped $Y_2O_3:Eu^{3+}$ (1mol %) Nanophosphors

Using a solution combustion method, $Y_2O_3$ nanophosphors co-doped with 1 mol % $Eu^{3+}$ and 1 mol % $Ca^{2+}$ were produced. This was achieved by dissolving yttrium nitrate [$Y(NO_3)_3 \cdot XH_2O$], Europium nitrate

hexahydrate [Eu $(NO_3)_3 \cdot 6H_2O$], Calcium nitrate tetrahydrate, and urea $[CO(NH_2)_2]$ in double-distilled water. The components were mixed in a stoichiometric ratio to form a homogeneous solution. After that, this solution was put in a silica crucible and heated in a preheated muffle furnace to 600°C for 15 minutes. The resulting foamy solid was then easily ground with an agate mortar to produce fine precursor powder, and it was annealed for two hours at 1000°C to improve crystallinity. The combustion process resulted in a frothy sample, which was subsequently ground into a fine powder for further characterization.

**Anticounterfiting ink**

In order to achieve the target dynamic viscosity, 50 mg of the $Y_2O_3$:$Eu^{3+}$ (1mol %), $Ca^{2+}$ (1mol %) is carefully dispersed into an ethanol- water solution at a ratio of 50:50. Then this mixture undergoes stirring with a magnetic stirrer at ~ 70°C until it became clear (approximately 10 min). Subsequently, to ensure thorough mixing, the appropriate volume of the PVA solution added. After that, 10 mL of deionized water was used to dissolve 1 gm of polyvinyl alcohol (PVA) with an average molecular weight of 125,000 g/mol for 10% solution and add to that prepared mixture. Also subjected 0.2 gm PEG- 200 (Polyethylene Glycol) in this followed by sonication for 30 min to achieve homogeneity. We obtained AC ink employed for printing AC patterns on various surfaces due to its high viscosity and polymeric composition. These patterns are subsequently observed in real-time while exposed to UV 365 nm light irradiation [19].

**Preparation of $Ca^{2+}$ co-doped $Y_2O_3$: $Eu^{3+}$ hydrogel.**

Chitosan with an 85% degree of deacetylation (dd) and 25% glutaraldehyde was used in this process. To proceed with the experiment, firstly, a chitosan solution was prepared by adding 1.7 g of chitosan powder to 1% aqueous acetic acid and left for 8-10 hours at ~50°C with continuous stirring to obtain a 1% (w/v) solution. The viscous and pale yellow chitosan solution was filtered to remove any undissolved particles. Added PEG-200 (2% v/v) and glycerine (1% v/v) to the chitosan solution and stirred until fully mixed (about 20 min). Disperse nanophosphors 60 mg (~0.2% w/v) into the chitosan mixture and ultrasonicate (5–10 minutes) to achieve uniform dispersion. Slowly added 0.25 ml glutaraldehyde (~0.25% v/v) dropwise while stirring, and the pH was between 4.5 and 6.5. Then wait for 1–2 hours at room temperature to allow Schiff base formation between chitosan amine groups and glutaraldehyde groups. After some time, a slightly yellow color was observed, indicating a reaction to occurred. Then, for desolvation, cold 2-propanol (~4°C) was chosen. Added the chitosan mixture dropwise into 2-propanol under stirring. Then, turbidity was observed immediately, which means phase separation and gel formation occurred, and for a clearer solution, it was separated by centrifugation. Let the gel particles remain undisturbed to form a bulk hydrogel structure. Wash the hydrogel 2–3 times with fresh cold 2-propanol to remove residual acetic acid and unreacted matter. Let the hydrogel place at 4°C for 12–24 hours to stabilize the network and store in distilled water at 4°C. At last, cast the mixture into molds to give any shape, and then we can observe the glowing red colour hydrogel through 365 nm UV light.

## MATERIALS CHARACTERIZATION

The Multipurpose Versatile XRD System (Smart Lab 3kW, Rigaku) was employed for both powder XRD analyses of $Ca^{2+}$ ions co-doped with $Y_2O_3$:$Eu^{3+}$ phosphor samples, scanning a 2θ range from 10° to 70° to

evaluate the structural and phase purity. The surface morphology of $Y_2O_3$: $Eu^{3+}$ and $Ca^{2+}$ activated phosphor samples was studied using a High-Resolution Field Emission Scanning Electron Microscope with EDS (FE-SEM) (JSM-7610F Plus, JEOL). The luminescence decay profiles for the entire series of $Y_2O_3$:$Eu^{3+}$ and $Ca^{2+}$ samples were recorded with a Quanta Master 8450-22 Spectrofluorometer (Horiba), which measures fluorescence across the UV-VIS-NIR range (~200 nm to 3000 nm).

## RESULT AND DISCUSSION

### XRD and Structural parameter evaluation

The X-ray diffraction patterns of the calcined $Y_2O_3$:$Eu^{3+}$ (1mol %), $Ca^{2+}$ (1mol %) doped nanophosphors are shown in Figure 1. The findings demonstrate that there are no discernible impurity peaks in the XRD patterns when compared to the typical JCPDS data. This shows that the trivalent Europium and Calcium ions have effectively integrated into the $Y_2O_3$ host without altering the crystal structure, and that the synthesized samples are single-phase.

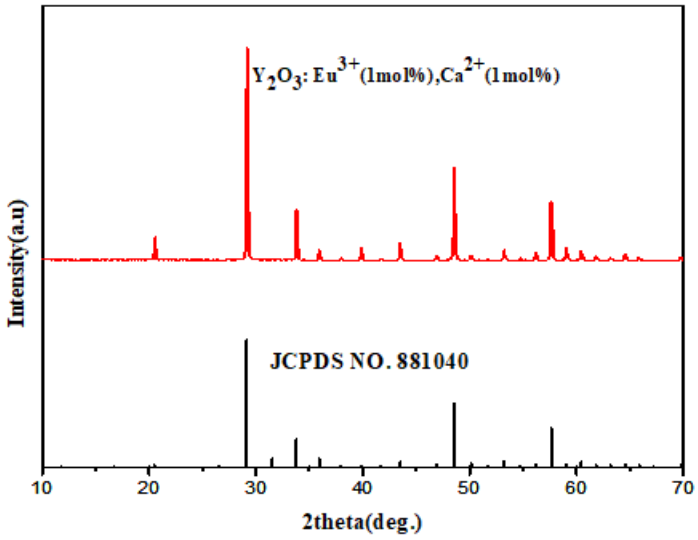


**Figure 1: shows the normal JCPDS data of the host Y2O3, as well as the powder X-ray diffractograms of $Y_2O_3$:$Eu^{3+}$ (1mol %) , $Ca^{2+}$ (1mol %) samples.**

The structural features, such as crystallite size, dislocation density, and microstrain, were ascertained using XRD data. As shown below, the crystallite size (D) nearly 80 nm was determined using the Hall-Williamsons equation (1) and the Debye-Scherrer's formula (2) [20,21,22].

$$\frac{\beta \cos\theta}{\lambda} = \frac{1}{D} + \frac{\epsilon \sin\theta}{\lambda} \quad (1)$$

$$D = \frac{0.9}{\beta \cos\theta} \quad (2)$$

$$\delta = 1 \div D^2 \quad (3)$$

$$\varepsilon = \beta \, \mathrm{Cos}\, \theta \div 4 \quad (4)$$

Here, ε stands for the macrostrain in the samples, D is the average crystallite size and β for the full-width at half-maximum (FWHM). Using the following relation in equation (3) and (4), the values of the microstrain (ε) and dislocation density (δ) were calculated as 6.848 and 1.55108E-07 respectively for $Y_2O_3$: $Eu^{3+}$ (1mol %), $Ca^{2+}$ (1mol %) nanophosphor.

**SEM**

A scanning electron microscope was used to analyse the synthesised phosphor powder's surface morphology and crystallite sizes. At 1000°C, a combustion procedure was used to complete the synthesis. This indicates that the combustion reactions of the mixes proceeded without any problems. Along with morphological images, Figure 2 (a–b) shows exemplary SEM micrographs of $Y_2O_3$:$Eu^{3+}$, $Ca2^{+}$ phosphor materials. The micrograph crystallite diameters vary from 90-120 nm and are of spherical shape. SEM images show that all of the produced compositions have nearly comparable crystallite sizes, with the average crystallite size falling within the nm.range.

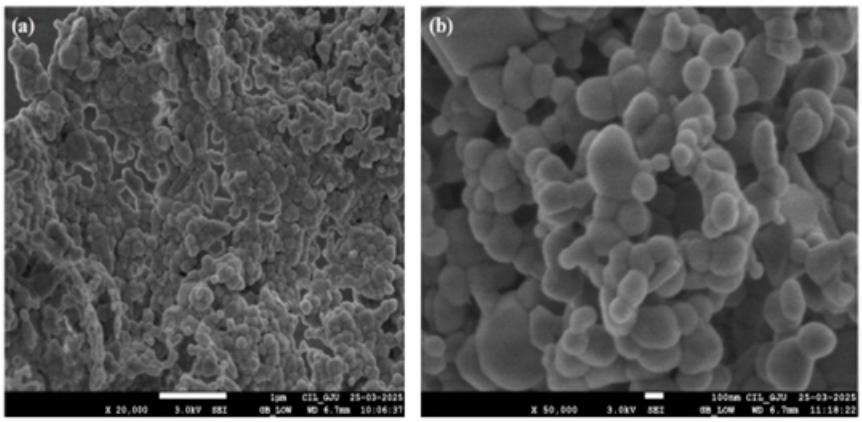


**Figure 2: (a–b) displays a typical SEM picture of the nanophosphor sample of $Y_2O_3$:$Eu^{3+}$ (1mol %), $Ca^{2+}$ (1mol %)**

**Photo-luminescence (PL) analysis:**

Figures 3 and 4 display the PL excitation and emission spectra of $Ca^{2+}$ (1 mol %) co-doped with $Y_2O_3$: $Eu^{3+}$ (1 mol %) nanophosphor, respectively. The PL excitation spectra of 1% $Eu^{3+}$ doped and $Ca^{2+}$ (1

mol %) co-doped with $Y_2O_3$ were recorded using the luminescence intensity as a function of the excitation wavelength. The detection wavelength was chosen at the primary peak of $Eu^{3+}$ at 613 nm, whereas the excitation wavelength was monitored between 320 and 600 nm as shown in Fig. 3. In this instance, the 230–260 nm range was observed where the charge transfer band was visible. The excited states of the $4f^6$ configuration and the $^7F_0$ ground state of $Eu^{3+}$ are the source of the transitions between 300 and 500 nm. The 4f-4f transitions of $Eu^{3+}$ ions are represented by the sharp peaks seen at 364 nm ($^7F_0 \rightarrow {}^5D_4$), 382 nm ($^7F_0 \rightarrow {}^5G_2$), 394 nm ($^7F_0 \rightarrow {}^5L_6$), 404 nm ($^7F_0 \rightarrow {}^5D_3$), 416 nm ($^7F_0 \rightarrow {}^5G_j$) and 466 nm ($^7F_0 \rightarrow {}^5D_2$), as well as a peak seen at 533 nm ($^7F_0 \rightarrow {}^5D_1$) that usually coincides with emission bands. [25].

As illustrated in Fig. 4, The PL emission spectra were recorded at an excitation wavelength of 348 nm and monitored in range 380–700 nm. The notable peaks of $Eu^{3+}$ were discovered at 581 nm with regard to the $^5D_0 \rightarrow {}^7F_0$, 588 nm and 594 nm with regard to the $^5D_0 \rightarrow {}^7F_1$, 613 nm with regard to the $^5D_0 \rightarrow {}^7F_2$ and its weak sub peak at 630 nm with same transition. In this instance, $Eu^{3+}$ ions were substituted in the lattice regions without an inversion centre, as indicated by the major signal for the $^5D_0 \rightarrow {}^7F_2$ transition at 613 nm. It is the main cause of the intense red colour [26]. Another peak is seen here at about 416 nm, which is probably caused by $Eu^{3+}$ 4f-4f transitions that originate from excited level $^5D_1$ the lower ground states. After calcium doping, the peak intensities increase by approx. 1.5 times, but the peak positions stay the same as in pure $Y_2O_3$: $Eu^{3+}$ nanophosphor. Figure 5 illustration depicting the process of energy transfer with $Ca^{2+}$ ions in $Y_2O_3$:$Eu^{3+}$ nanophosphors.

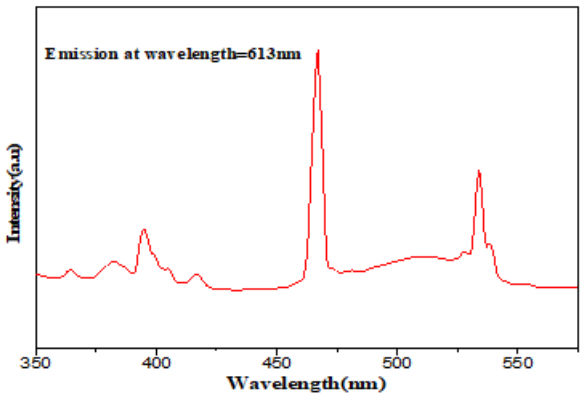


**Figure 3: PL excitation of the $Y_2O_3$:$Eu^{3+}$ (1mol %), $Ca^{2+}$ (1mol %) nanophosphor at λem = 613 nm.**

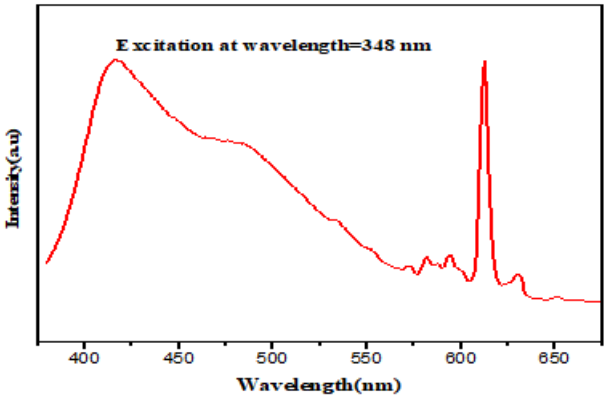


**Figure 4: The $Y_2O_3:Eu^{3+}$ (1mol %) , $Ca^{2+}$ (1mol %) nanophosphor PL emission spectra at λex = 348 nm**

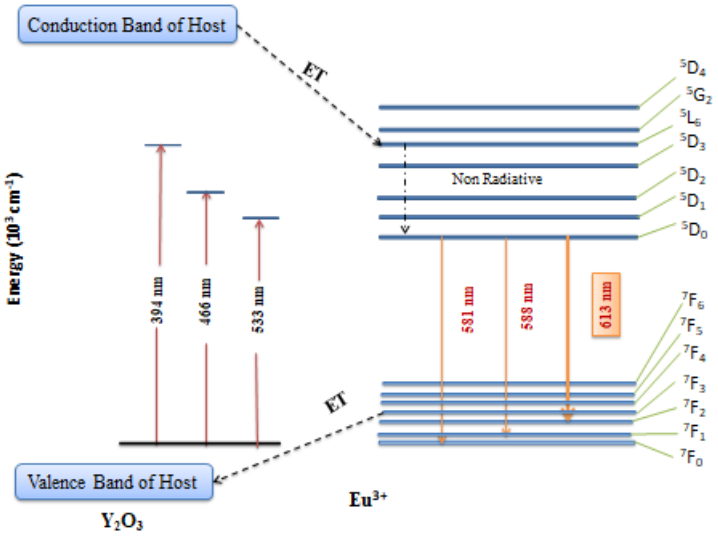


**Figure 5: Illustration depicting the process of energy transfer with $Ca^{2+}$ ions in $Y_2O_3$: $Eu^{3+}$ nanophosphors.**

**Evaluation of CIE parameters**

For $Y_2O_3:Eu^{3+}$ and $Ca^{2+}$ co-doped $Y_2O_3:Eu^{3+}$ phosphors, the CIE coordinates and correlated colour temperature (CCT) were analysed. The examination of the CIE coordinates (x=0.63, y=0.36) and the outcomes are displayed in Fig. 6. By calculating the colour correlated temperatures (CCTs), the nature of colour emission was investigated. The following McCamy empirical equation (3) was used to determine CCT.

$CCT(x,y)= 437n^3+3601n^2 - 6861n+5514931(3)$ where n is the ratio of (x−xe) to (y−ye), and xe = 0.3320 and ye = 0.1858.6 [33, 34]. The CCT graphs for the $Ca^{2+}$ (1mol %) co-doped $Y_2O_3:Eu^{3+}$ (1mol %) phosphor are shown in Figure 7. The CCT values is 2130K. Consequently, the manufactured samples' CCT

values show a cool white light output.

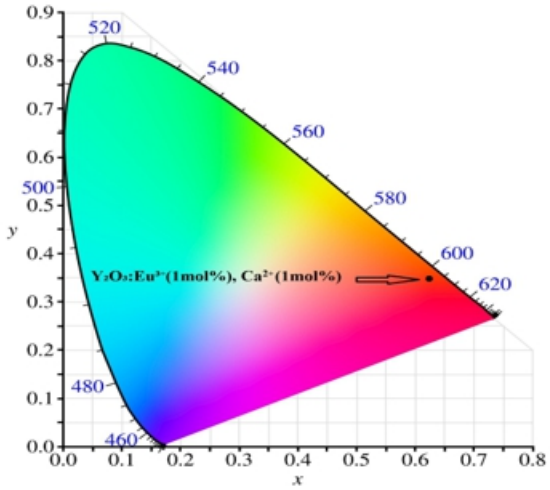


**Figure 6: CIE Colour coordinates of $Y_2O_3$:$Eu^{3+}$ (1mol %), $Ca^{2+}$ (1mol %).**

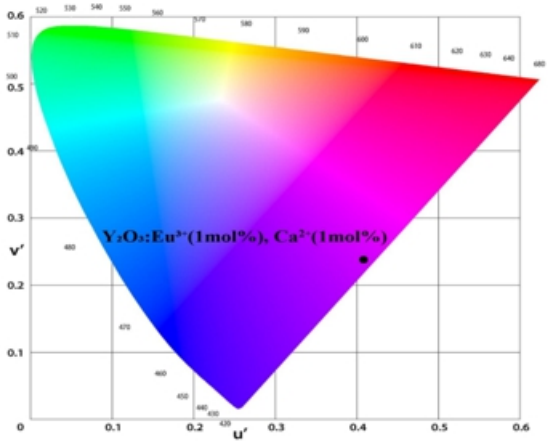


**Figure 7: $Y_2O_3$:$Eu^{3+}$ (1mol %), $Ca^{2+}$ (1mol %) u' and v' diagram**

## APPLICATIONS

### Applications of data security

The exceptional photoluminescent characteristics of the $Y_2O_3$:$Eu^{3+}$, $Ca^{2+}$ nanocomposites created in this work offer promising prospects for real-world data encrypting applications. Society has always placed a high value on data protection and preservation, but creating sophisticated chemical anti-counterfeiting (AC) systems is fraught with difficulties. In an attempt to stop counterfeiting, a variety of fluorescent materials have been employed; nevertheless, problems with toxicity, spectral overlap, low quantum efficiency, and luminescence quenching remain. It's difficult to make AC ink that prevents security documents from being forged. Figure 8a shows AC labels created using $Y_2O_3$:$Eu^{3+}$, $Ca^{2+}$ composite on various surfaces. The

images created using a basic brush technique on a variety of media (metal, glass, wood, aluminium paper, and cardboard) are shown in Figure 8(a).

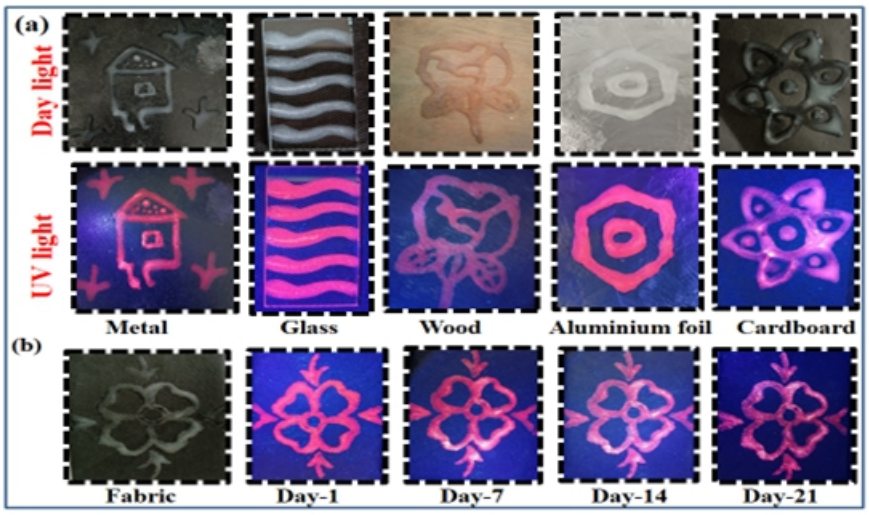


**Figure 8: (a) AC labels displayed on various surfaces (b) Extended storage period on Fabric**

Both natural light and UV 365 nm light are used to observe these AC labels, which were created on various surfaces. Under typical lighting conditions, the patterns exhibit clear, sharp luminescence that is invisible to the human sight. These outcomes demonstrate how useful the developed ink is for data encrypting applications involving UV source. When exposed to UV light at 365 nm, the AC patterns on various substrates produce a vivid red hue that is undetectable during the day. The emission colour stayed the same even after 21 days, demonstrating the longevity of the $Y_2O_3:Eu^{3+}$, $Ca^{2+}$ ink and its suitability for safe applications. This is demonstrated in Fig. 8(b), which evaluates the stability of the AC patterns over time at room temperature (1–21 days). The designs created by AV ink on glass surface were treated with several solvents, including ethanol, acetone, HCl, $NH_3$, and NaOH, in order to assess the ink's chemical stability. The digital images displayed in Fig 9 demonstrate the patterns' notable resistance to all the above mentioned solvents.

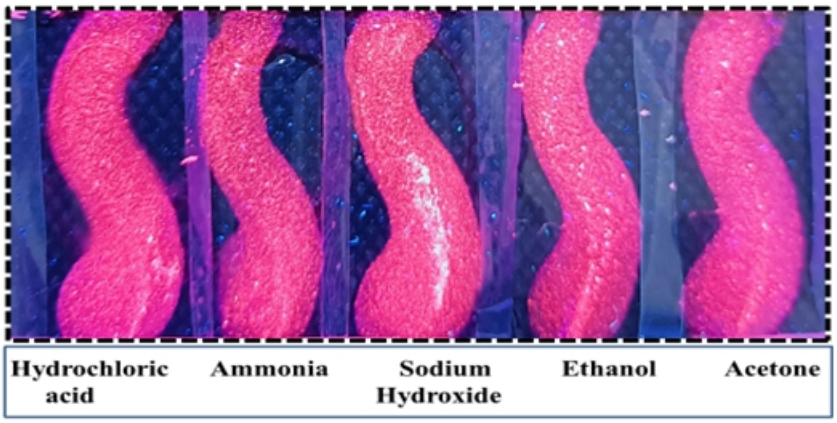


**Figure 9: AC label solvent treatment with different solution in the presence of UV light at 365nm.**

**Hydrogels with light properties**

The capability to create luminescent hydrogels that function under both daylight and UV light conditions provides considerable flexibility in the development of advanced photonic and optoelectronic materials. Fig.10 shows luminescent hydrogels observed under day light and UV light at 365 nm. In daylight, the hydrogel is transparent and flexible, making it easy to handle and compatible with biological or environmental systems. When exposed to UV light, the embedded $Ca^{2+}$ co-doped $Y_2O_3$: $Eu^{3+}$ phosphors emit a bright red light, which facilitates real-time visualization, encoding, and optical applications [27, 28]. This dual functionality makes the hydrogel particularly well-suited for various multifunctional uses, including UV-activated biosensors, anti-counterfeiting materials, photo-switchable coatings, and smart displays. Additionally, the luminescence triggered by UV light enables non-contact, remote activation, paving the way for new opportunities in optical communication and responsive systems in soft materials.

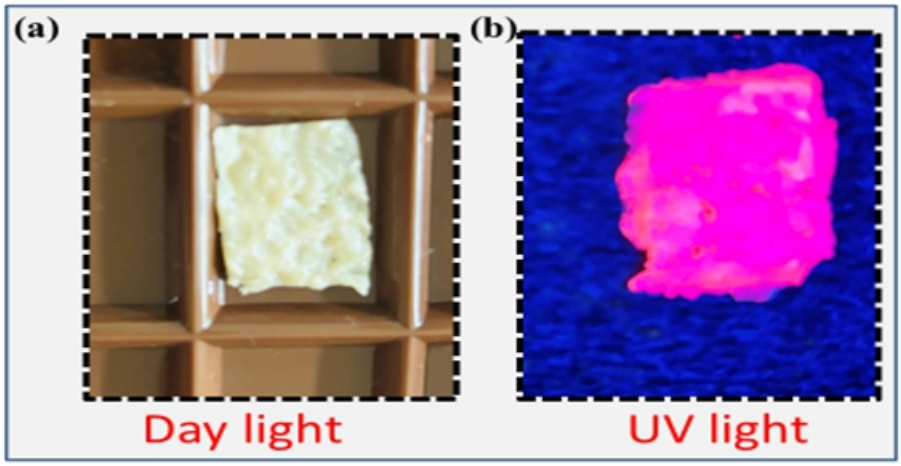


**Figure 10: (a) Hydrogels observed under Day light (b) UV light at 365 nm**

## CONCLUSION

In summary, $Ca^{2+}$ co-doped $Y_2O_3$: $Eu^{3+}$ nano-phosphors that emit cool white light were synthesized using a urea-assisted solution-combustion method. XRD analysis confirmed phase purity, while results indicated that the crystallites exhibit a semi-spherical shape with dimension 80 nm. SEM images revealed that the morphology of $Y_2O_3$ co-doped with Europium and Calcium ions was seems to be largely uniform and primarily spherical, demonstrating successful synthesis of the nanophosphors, effective incorporation of $Eu^{3+}$ and $Ca^{2+}$ ions within the $Y_2O_3$ matrix without significant phase separation. No major morphological changes were observed due to co-doping, suggesting the dopants do not materially alter the overall microstructure. These features confirm that the synthesized material maintains its structural integrity while accommodating the dopants. The optimized $Y_2O_3$:$Eu^{3+}$ (1 mol%) and $Ca^{2+}$ (1 mol%) phosphor displayed CIE coordinates which are near the NTSC red standards, along with a high correlated color temperature of 2130 K, suggesting it emits a cool white light. These findings underscore its potential for use as a cool-emitting phosphor in near-UV excited red LED applications. Photoluminescence showed that $Ca^{2+}$ co-doping increased charge compensation and decreased non-radiative losses, resulting in enhanced red emission at 613 nm ($^5D_0 \rightarrow {}^7F_2$ transition). $Ca^{2+}$ doped $Y_2O_3$: $Eu^{3+}$ nanophosphors are hence attractive for red components in solid-state and optoelectronic lighting applications. The optimized NCs are utilized to

produce AC labels on different substrates. The resulting AC images exhibit high sensitivity and improved contrast, thanks to their superior fluorescence properties and binding specificity. Overall, the results clearly indicate that the enhanced nano-luminous material hold significant promise for applications in anti-counterfeiting and hydrogel.

## References

1. Kostyukov A.I. et al.(2024).Photoluminescent Y2O3:Eu3+@PVA composite dispersions and films for anti-counterfeiting ink applications, Optical Materials,157,116194
2. Binnemans K. et al. (2005). Interpretation of europium (III) spectra. Coordination Chemistry Reviews, 295, 1–45.
3. Blasse G. & Grabmair B.C. (1994) Luminescent Materials. Springer, Chapter 1,1-9.
4. Dhananjaya N., et al. (2017). Enhanced red emission in $Eu^{3+}$ doped $Y_2O_3$ nanophosphors. Materials Research Bulletin, 89, 265–271.
5. Zhang X., et al. (2012). Influence of $Ca^{2+}$ co-doping on luminescence of $Y_2O_3:Eu^{3+}$. Optical Materials, 34, 1818–1823.
6. Kumar S. & Rai S. B. (2008). Effect of $Ca^{2+}$ ions on photoluminescence properties of $Y_2O_3:Eu^{3+}$ nanophosphors. Journal of Applied Physics, 104, 103519.
7. Zheng F., et al. (2011). Role of $Ca^{2+}$ co-doping in improving the luminescence of $Y_2O_3:Eu^{3+}$ phosphors. Journal of the American Ceramic Society, 94, 4104–4110.
8. Zhuang Y. X., et al. (2015). Influence of co-dopants on crystal field and site symmetry in $Y_2O_3:Eu^{3+}$ phosphors. Journal of Rare Earths, 33, 755–762.
9. Li Y., et al. (2017). Rare-earth-doped luminescent materials for anti-counterfeiting applications. Advanced Optical Materials, 5, 1700481.
10. Wang F., & Liu, X. (2009). Recent advances in the chemistry of lanthanide-doped upconversion nanocrystals. Chemical Society Reviews, 38, 976–989.
11. Zhang F., et al. (2011). Influence of $Ca^{2+}$ co-doping on luminescence of $Y_2O_3:Eu^{3+}$. Journal of the American Ceramic Society, 94, 4104–4110.
12. Kumar S., & Rai, S. B. (2008). Enhanced luminescence in $Y_2O_3:Eu^{3+}$ nanoparticles with $Ca^{2+}$ co-doping. Journal of Applied Physics, 104, 103519.
13. Zhuang Y. X., et al. (2015). Role of co-dopants in tuning site symmetry of $Y_2O_3:Eu^{3+}$ phosphors. Journal of Rare Earths, 33, 755–762.
14. Gai S., et al. (2014). Recent advances in functional nanomaterials for anti-counterfeiting. Nanoscale, 6, 4653–4663.

15. Yang Y., et al. (2018). Fluorescent hydrogels for wearable anti-counterfeiting applications. ACS Applied Materials & Interfaces, 10, 34518–34525.

16. Gao M., et al. (2020). Responsive hydrogels as smart anti-counterfeiting materials. Advanced Functional Materials, 30, 2004328.

17. Hu Z., et al. (2021). Smart hydrogels for optical anti-counterfeiting: From stimuli response to encryption and decryption. Chemical Engineering Journal, 426, 131905.

18. Zhao Q., et al. (2020). Biocompatible luminescent hydrogels: A platform for bio-imaging and security printing. Materials Horizons, 7, 1017–1035.

19. Mamatha G.R. et al. (2023). Designing ultra-highly efficient Sm3+activated SrLaAlO4 orange-red emitting phosphor towards security encoding, hydro-gels, flexible displays and personal identification, Journal of Photochemistry and Photobiology A: Chemistry, 445,115087

20. Chen Z. et al. (2009). Microwave induced solution combustion synthesis of nano-sized phosphors, Journal of Alloys and Compounds, 473, 13–16.

21. Singh P. et al. (2008). In situ high temperature XRD studies of ZnO nanopowder prepared via cost effective ultrasonic mist chemical vapour deposition. Bulletin of Materials Science, 31,573-577.

22. Jayaram P. et al. (2016). Micro-strain, dislocation density and surface chemical state analysis of multication thin films, Physica B: Condensed Matter, 501, 140-145

23. Renuka L. et al. (2021). Phase-transformation synthesis of Li codoped ZrO2:Eu3+ nanomaterials: characterization, photocatalytic, luminescent behaviour and latent fingerprint development Ceramics International, 47, 10332-10345.

24. Sun M.et al. (2020). Effect of Zn2+ and Li+ ions doped on microstructure and upconversion luminescence of Y2O3:Er3+-Yb3+ thin films, Journal of Alloys and Compounds, 816, 152575.

25. Zhao T.et al. (2023). Enhanced effect of co-doping of Ln3+on the luminescent properties of BaSiO3:Eu3+red phosphors, Physica B: Condensed Matter, 661, 414921

26. Yousif A et al. (2015). Comparison and analysis of Eu3+ luminescence in Y3Al5O12 and Y3Ga5O12 hosts material for red lighting phosphor, Materials Chemistry and Physics,166, 167-175

27. Guangyou L. et al. (2023). Flexible, stretchable, and luminescent hydrogels based on a polydimethylsiloxane-coated CsPbBr3 nanostructure for elastomers, ACS Applied Nano Materials, 11, 9588–9597.

28. Qingdi Z. et al. (2018). White light-emitting multistimuli-responsive hydrogels with lanthanides and carbon dots, ACS Applied Materials & Interfaces, 12, 10409–10418.